analytical chemistry

pubs.acs.org/ac

Letter

Structural- and Site-Specific *N*-Glycosylation Characterization of COVID-19 Virus Spike with StrucGP

Bojing Zhu, Zexuan Chen, Jiechen Shen, Yintai Xu, Rongxia Lan, and Shisheng Sun*

Cite This: *Anal. Chem.* 2022, 94, 12274−12279

Read Online

ACCESS | Metrics & More | Article Recommendations | Supporting Information

ABSTRACT: The spike (S) protein plays a key role in COVID-19 (SARS-CoV-2) infection and host-cell entry. Previous studies have systematically analyzed site-specific glycan compositions as well as many important structural motifs of the S protein. Here, we further provide structural-clear *N*-glycosylation of the S protein at a site-specific level by using our recently developed structural- and site-specific *N*-glycoproteomics sequencing algorithm, StrucGP. In addition to the common *N*-glycans as detected in previous studies, many uncommon glycosylation structures such as LacdiNAc structures, Lewis structures, Mannose 6-phosphate (M6P) residues, and bisected core structures were unambiguously mapped at a total of 20 glycosites in the S protein trimer and protomer. These data further support the glycosylation structural−functional investigations of the COVID-19 virus spike.

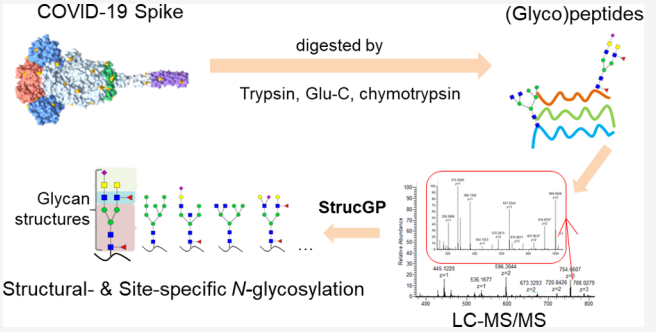

The COVID-19 pandemic has caused millions of deaths worldwide. The spike (S) protein on the surface of the severe acute respiratory syndrome coronavirus 2 (COVID-19 or SARS-CoV-2) virus contains 22 potential N-linked glycosylation sites per protomer (expressed in human cells) and plays essential roles during COVID-19 infection and host-cell entry.[1−5] The viral glycans, which are fully synthesized by the host glycosylation biosynthesis system, can help the virus escape the host immune response.[6] Due to the fact that different glycan structures (instead of glycan compositions) at different glycosites may have distinctive functions,[7,8] the systematical analyses of viral glycans at both structural- and site-specific levels are essential for bringing new insights to immune evasion and vaccine promotion.

In previous studies, the glycan compositions at each glycosite of the S protein have been systematically analyzed.[1,6,9−18] Some structural motifs on the S protein such as LacdiNAc and Mannose 6-phosphate (M6P) have also reported previously.[12,16] The structural information on *N*-glycan released from the receptor binding domain (RBD) without glycosite information has also been investigated.[19,20] In this study, we further characterized additional structural features of *N*-glycans at each glycosite of the COVID-19 virus S protein (both trimer and protomer expressed in HEK293 cells) by using our recently developed glycopeptide interpretation software, StrucGP.[21]

The protein samples were digested into peptides using three individual enzymes followed by triplicate LC-MS/MS analyses of each peptide sample with two fragmentation energies (low and high HCD energies) on each glycopeptide peak.[21] Using StrucGP, a total of 304 *N*-glycans with distinct structures attached at 19 *N*-glycosites (1307 unique N-linked intact glycopeptides) were identified from the S trimer within 1% false discovery rates (FDR < 1%) at both peptide and glycan levels (Figures S1 and S2 and Table S1). These glycan structures identified by StrucGP could be further sorted into 135 unique *N*-glycan compositions. In fact, glycan isoforms were detected at 17 glycosites (Figure S3a and Table S2), and one single composition, such as N4H5F1, could have up to nine distinct structural isoforms (Figure S3b, c). Notably, glycans with uncommon structures were distinguished from their isomers, which have not been or just partially achieved in previous studies (Figure S2).

Based on our modular strategy as described in StrucGP, these *N*-glycan structures could be divided into four types of core structures and 11 branch structures with three glycan subtypes (Figure 1A). Among four types of core structures, the fucosylated core structures (with and without bisected GlcNAc), which were detected at all 19 identified glycosites, accounted for almost two-thirds of all site-specific glycans (Figure 1B). The core-fucosylation rates were greater than 50% at eight glycosites and greater than 30% at another seven glycosites. This is almost the same as previous studies on the HEK293 expressed S RBD, except that we only identified one (glyco)peptide-spectra match (PSMs) at N343.[14] The common

Received: May 27, 2022
Accepted: August 23, 2022
Published: August 29, 2022

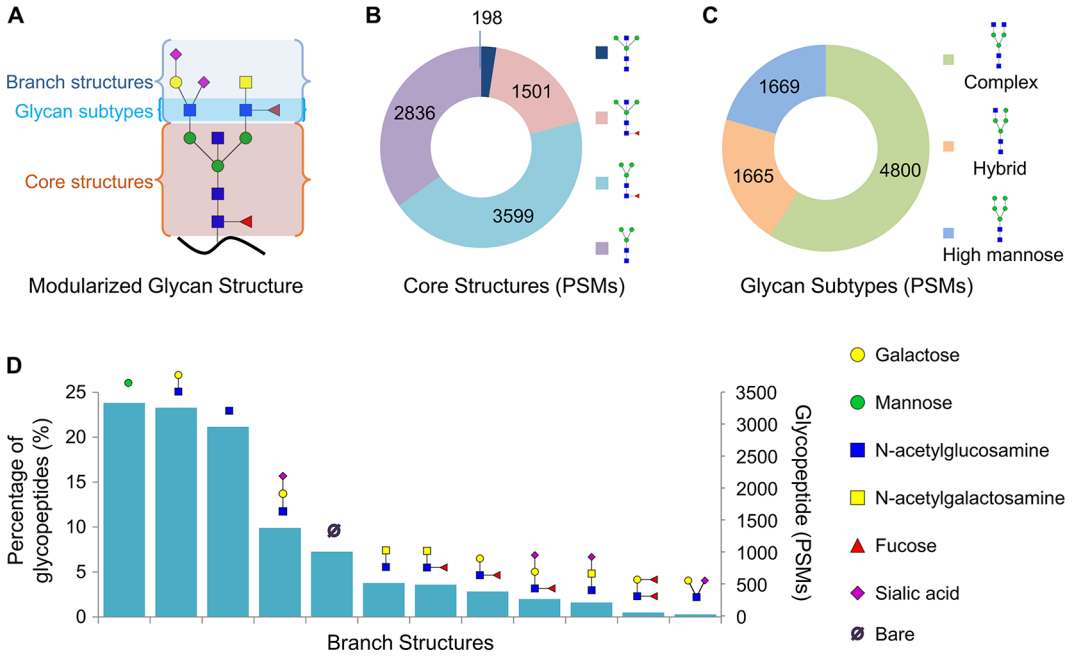

Figure 1. Overall glycosylation characteristics of COVID-19 virus spike protein trimer. (A) *N*-glycan structures were divided into core structures, glycan subtypes, and branch structures. (B–D) Distributions of core structures (B), glycan subtypes (C), and branch structures (D) on IGPs of the S trimer.

core structure HexNAc2Hex3 accounted for 34.9%, and the bisected core structure without fucose (HexNAc3Hex3) accounted for the remaining small portion. In terms of glycan subtypes, complex glycans occupied approximately 59% of all glycans on intact glycopeptides (IGPs) based on PSMs, while high-mannose and hybrid subtypes each accounted for around one-fifth (Figure 1C). The complex-type glycans were divided into nearly four-fifths biantennary and one-fifth triantennary glycans based on their PSMs. Besides, there were only 3.62% tetraantennary and two pentaantennary PSMs (Figure S4). It should be noted that as the poly-LacNAc structures could not be distinguished by StrucGP any existing poly-LacNAc would eventually be identified as multiantennary glycans. Among 11 distinct branch structures, simple structures such as oligo-mannose, LacNAc (Hex-HexNAc), and single HexNAc were most abundant, followed by sialyl LacNAc (NeuAc-Hex-HexNAc) and an empty branch (Figure 1D). The remaining branch structures were only present in a minor proportion. Nevertheless, these low-existing branch structures contain a number of uncommon and distinctive glycan structures that have the potential to perform special biological functions.

Glycan structures on the S trimer showed apparent heterogeneities among different glycosites (Figure 2). Glycosites N282, N616, N801, N1074, and N1098 were modified by a variety of glycans, with common branch structures such as empty branch, oligo-mannose, single HexNAc, LacNAc, and sialyl LacNAc predominating. Aside from these common branches, there were also a few Lewis structures such as (sialyl-)Lewis$^{x/a}$ (Gal-(Fuc-)GlcNAc) and Lewis$^{y/b}$ (Fuc-Gal-(Fuc-)GlcNAc), as well as LacdiNAc (GalNAc-GlcNAc) structures with and/or without sialic acid and fucose at the glycosites N74, N122, N149, and N165. Only a few glycans were identified at the glycosites N343, N1134, and N1173. As for glycosites N17, N61, N234, and N603, they were mainly modified by common-branched glycans, among which the oligo-mannose branch structure occupied the most. There results were consistent with the glycosylation heterogeneities among glycosites as reported in a previous study.[18] In particular, 93.6% of the glycans at N234 were high-mannose type, which was consistent with the glycosylation of different S protein samples from five different laboratories and a virus strain.[17] One possible reason is that narrow space surrounding this site hinders elongated glycans since the site of N234 is facing inward between spike protomers. There is no evidence to support that glycosylation heterogeneities among glycosites are domain dependent.

Special or uncommon glycosylation is generally linked to specialized functions, which are critical for important biological processes.[22−25] However, due to the limitations of technologies for analyzing site-specific *N*-glycan structures on specific proteins, the functions of these structures are mostly unknown. By using StrucGP, glycans containing special (sialylated or fucosylated) LacdiNAc structures, Lewis structures (including Lewis$^{x/a/y/b}$ with or without NeuAc), NeuAc-(Gal-)GlcNAc branches, M6P residues, and bisected glycans were unambiguously characterized at different glycosites (Figure 3 and Table S3). We applied an oxonium ions-triggered HCD MS/MS with two different fragmentation energies to acquire reliable glycopeptides MS2 spectra. Structural- and site-specific glycosylation were characterized via characterizing a series of glycan feature B ions with their corresponding glycopeptide Y ions at a low HCD energy and peptide b/y ions at a high HCD energy (Figures S5−S9).

After excluding glycopeptides with only one PSM (PSMs ≥ 2), 59 LacdiNAc-containing *N*-glycans modified at seven glycosites (99 unique glycopeptides) were identified from the N-terminal domain (NTD) and RBD of the S trimer (Figure 3). Among them, glycopeptides containing solely LacdiNAc (GalNAc-GlcNAc) and/or fucosylated LacdiNAc (GalNAc-(Fuc-)GlcNAc) accounted for approximately three-eighths of the total, while glycopeptides containing sialylated LacdiNAc (NeuAc-GalNAc-GlcNAc) accounted for nearly a quarter. In

https://doi.org/10.1021/acs.analchem.2c02265
Anal. Chem. 2022, 94, 12274−12279

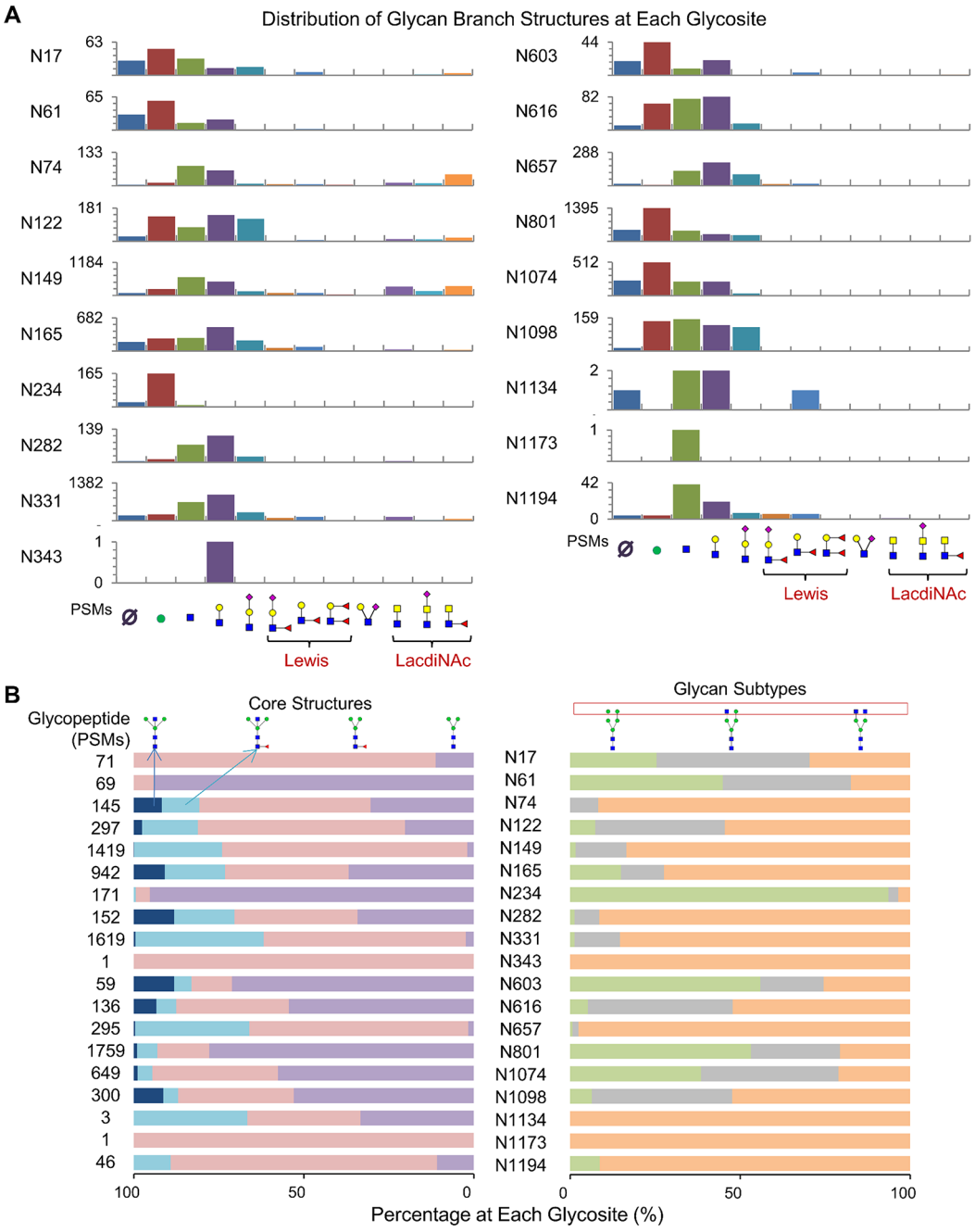

Figure 2. Precise structural analysis of site-specific *N*-glycans from COVID-19 spike trimer. (A) Distribution of branch structures, (B) core structures (left), and glycan subtypes (right) of glycans on each glycosite of the S trimer.

fact, the feature B ion at m/z 407 for LacdiNAc has been detected on the S trimer in a previous publication by Zhao et al.,[26] although the glycan was finally assigned to a different glycan structure just based on its composition. A total of 50 glycans with Lewis structures were identified at 10 glycosites (84 unique glycopeptides), including Lewis$^{x/a}$ structures at all 10 sites and sialylated Lewis$^{x/a}$ structures at six sites, while Lewis$^{y/b}$ structures were identified at four glycosites within the NTD and RBD regions. It should be noted that further confirmation steps are still needed for these Lewis structures as the fucose migration has not been entirely overcome.[27] In addition, seven different glycans containing uncommon NeuAc-(Gal-)GlcNAc structures were identified at the glycosites N149, N331, and N801. Sialic acid attached to the GlcNAc structure was determined by the combination of its characteristic B ions (m/z 495.18, z = 1) and the corresponding Y ions (Figure S8). This atypical sialylated glycan has been demonstrated in human samples in several previous studies.[28,29] Remarkably, two unique M6P-containing glycans were also detected at the glycosite N149 (PSMs ≥ 2), which was consistent with a recent study by Huang et al.,[16] in which M6P glycopeptides have also been reported on HEK293 expressed S protein. As for core structures, the bisected cores as well as the bisected-fucosylated cores were determined at 13 glycosites with 1609 (20.4%) glycopeptide spectra. The bisecting *N*-glycan is known to serve as a suppressor of *N*-glycan elongation and is involved in cell growth control and tumor progression and is highly relevant to the nervous system.[23−25] As described above, these special or uncommon glycan structures

https://doi.org/10.1021/acs.analchem.2c02265
Anal. Chem. 2022, 94, 12274−12279

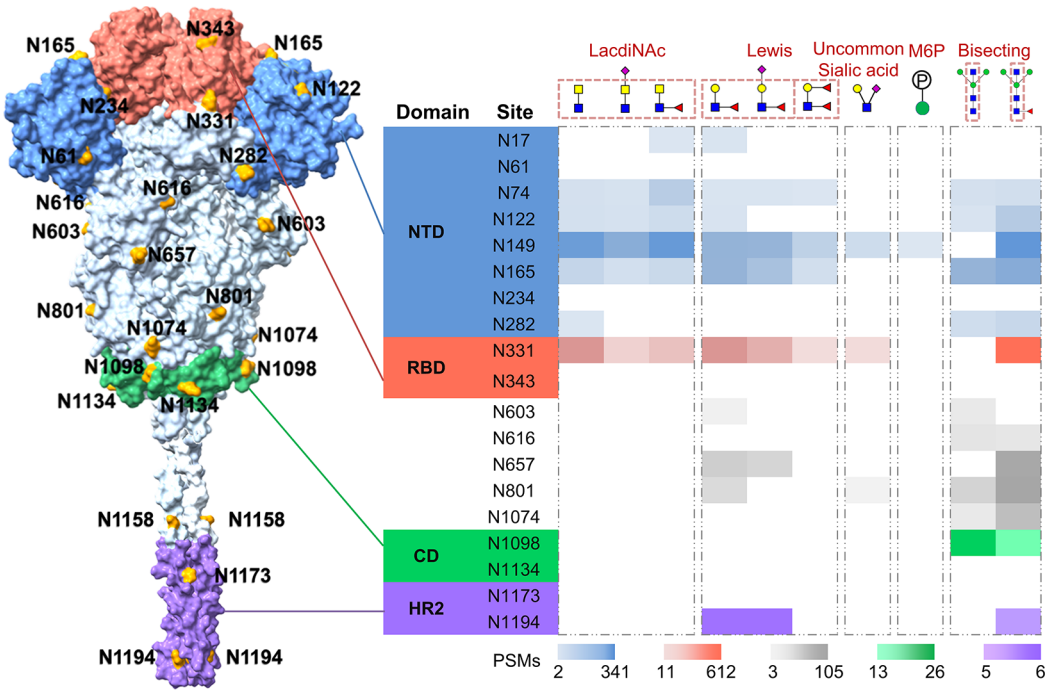

Figure 3. Trimeric model displaying the site-specific uncommon glycosylation of the COVID-19 spike (glycopeptide PSMs ≥ 2). Detailed information can be found in Table S3. A description of the protein molecular modeling can be found in the Supporting Information. NTD, N-terminal domain; RBD, receptor binding domain; CD, connector domain; HR2, heptad repeat 2; M6P, Mannose 6-phosphate.

mainly occurred in the NTD and RBD (Figure 3), which may play important roles in regulating viral infection and receptor recognition. These data provide solid foundations for further investigating the biological functions of these special glycans.

We also characterized structural- and site-specific *N*-glycosylation on the S protomer. Overall, 1943 unique N-linked intact glycopeptides were identified from the S protein protomer, including 332 unique *N*-glycan structures (158 compositions) unambiguously assigned to 19 *N*-glycosites (Table S4). After filtering the results by using at least two PSMs per glycopeptides, we compared the differences of site-specific glycans between the protomer and trimer of the S protein (Figure 4). In comparison to the trimer, the protomer has more complicated and uncommon/special glycan structures. First, the protomer had more LacdiNAc structures (with/without sialylation and branch fucosylation) than the trimer. LacdiNAc structures were detected on 16 glycosites of the S protomer, a 1.3-fold increase to the S trimer, which is approximately consistent with the data obtained by Sanda et al.[12] Then, the proportion of Lewis structures on the protomer (14.39%) was higher than that of the trimer (9.36%). More Lewis$^{x/a}$ and sialylated Lewis$^{x/a}$ glycans were detected in the protomer than in the trimer. Glycans consisting of Lewis$^{y/b}$ structures were also detected at eight glycosites in the protomer compared with four glycosites in the trimer. Furthermore, NeuAc-(Gal-)GlcNAc-containing glycans were identified at five glycosites, two more than the trimer (N122 and N165). What is more special is that NeuAc-Gal-(NeuAc-)GlcNAc branches were newly determined in the monomer at N165 with six PSMs of N5H4S2F1-attached glycopeptides (Figure S8a). In contrast, common glycosylation branch structures (including empty branch, oligo-mannose, single HexNAc, LacNAc and sialyl LacNAc) in the protomer were declined by nearly 5% compared to the trimer. Furthermore, M6P residues were also detected at three more glycosites (N74, N1158, and N1194) in the protomer than in the trimer (Figure 4C). As for glycan subtypes, the percentage of complex-type glycans increased approximately one-sixth in the protomer than in the trimer (75% in protomer vs 59% in trimer), whereas high-mannose (21% vs 10%) and hybrid types (20% vs 15%) declined (Figure 4B). As to core structures, fucosylated cores were occupied more in the protomer than in the trimer (56.5% vs 44.6%), whereas the common HexNAc2Hex3 cores decreased more in the protomer than that in the trimer (21.8% vs 35.1%). The bisected cores as well as the bisected-fucosylated cores increased a little (Figure 4A). Overall, the S protomer comprised more complicated *N*-glycans than the trimer presumably because these glycans synthesized in the protomer had a less steric hindrance than the trimer and thus were able to conduct further *N*-glycan antennae elongation. Analogously, the protomer has a much lower level of high-mannose glycans than the trimer. This has also been observed on the HIV envelope protein, and its glycosylation has been shown to be constrained by its trimerization structure since steric constraints prevent the glycans from being recognized by glycosidases and glycosyltransferases.[30,31]

In summary, this study profiled structural- and site-specific *N*-glycosylation on the COVID-19 virus S protein with our newly developed software, StrucGP. Glycan structure isoforms as well as special/uncommon glycan structures were also precisely interpreted at site-specific levels. It should be mentioned again that as the real left or right branches of given glycans could not be determined by StrucGP, the structural motifs of *N*-glycans shown here were not the literal "structure" as confirmed in glycomics. In addition, as for some coeluting glycopeptide spectra, the current StrucGP can only report one major glycopeptide. Even though, the site-specific glycan structural information on S protein could still provide a solid foundation for further glycosylation functional investigations. During these analyses, StrucGP can serve as a valuable tool for structural- and

https://doi.org/10.1021/acs.analchem.2c02265
Anal. Chem. 2022, 94, 12274−12279

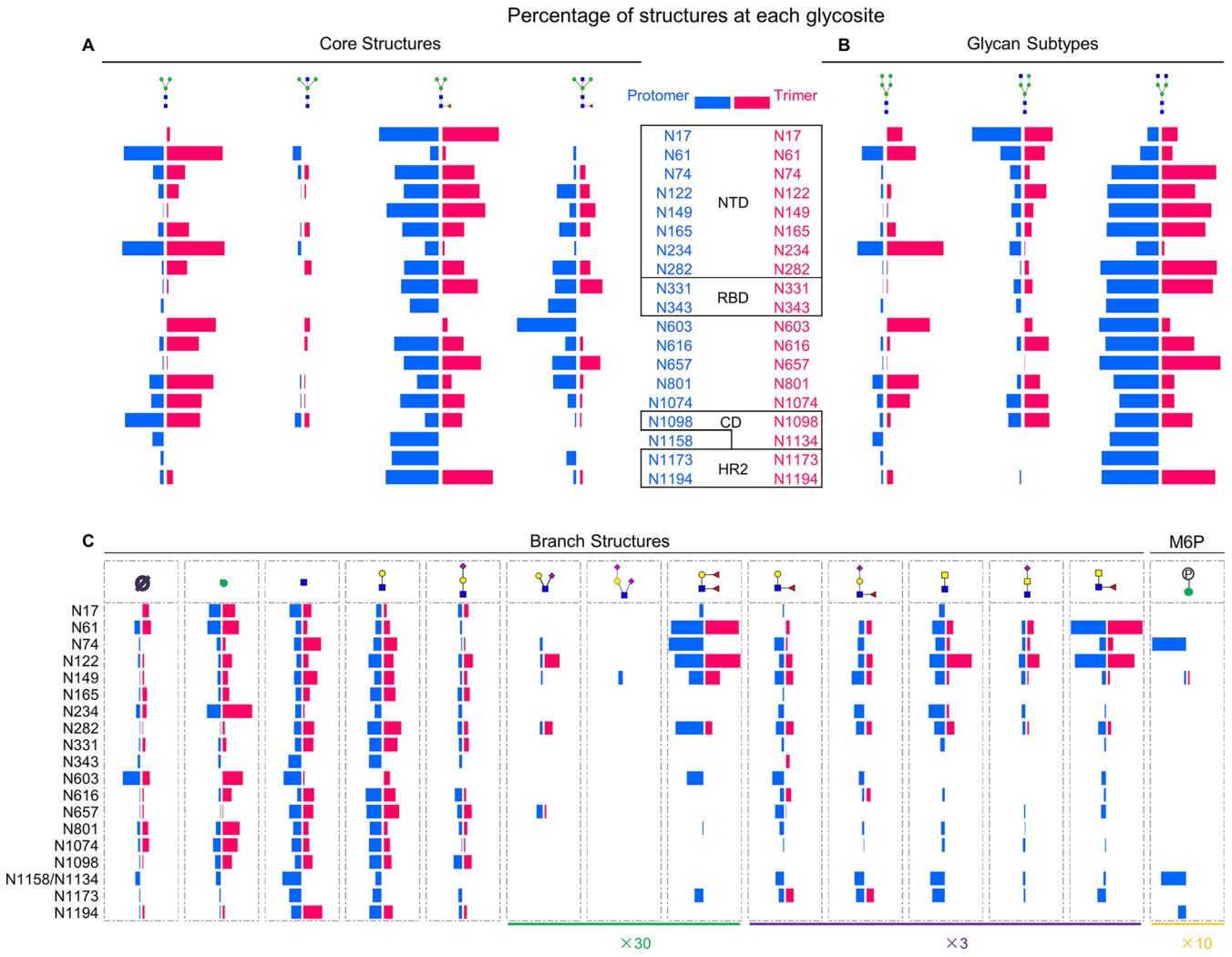

Figure 4. Glycosylation contrast of core structures (A), glycan subtypes (B), and branch structures (C) at each glycosite of the S protein between the protomer and trimer. NTD, N-terminal domain; RBD, receptor binding domain; CD, connector domain; HR2, heptad repeat 2; M6P, mannose 6-phosphate.

site-specific *N*-glycan interpretation for the expressed glycoproteins as well as the cell expression systems.

■ ASSOCIATED CONTENT

Supporting Information

The Supporting Information is available free of charge at https://pubs.acs.org/doi/10.1021/acs.analchem.2c02265.

Additional experimental details and supporting figures (PDF)

Table S1: Intact glycopeptides identified from HEK293 expressed COVID-19 Spike trimer by StrucGP (XLSX)

Table S2: Glycan compositions with different glycan isoforms identified in S trimer (XLSX)

Table S3: Heat map of uncommon site-specific glycans with PSM ≥ 2 in S trimer(XLSX)

Table S4: Intact glycopeptides identified from HEK293 expressed COVID-19 spike protomer by StrucGP (XLSX)

■ AUTHOR INFORMATION

Corresponding Author

Shisheng Sun − *College of Life Sciences, Northwest University, Xi'an, Shaanxi Province 710069, China;* orcid.org/0000-0002-7242-7164; Email: suns@nwu.edu.cn

Authors

Bojing Zhu − *College of Life Sciences, Northwest University, Xi'an, Shaanxi Province 710069, China*

Zexuan Chen − *College of Life Sciences, Northwest University, Xi'an, Shaanxi Province 710069, China*

Jiechen Shen − *College of Life Sciences, Northwest University, Xi'an, Shaanxi Province 710069, China*

Yintai Xu − *College of Life Sciences, Northwest University, Xi'an, Shaanxi Province 710069, China*

Rongxia Lan − *College of Life Sciences, Northwest University, Xi'an, Shaanxi Province 710069, China*

Complete contact information is available at: https://pubs.acs.org/10.1021/acs.analchem.2c02265

Author Contributions

The manuscript was written through contributions of all authors. All authors have given approval to the final version of

https://doi.org/10.1021/acs.analchem.2c02265
Anal. Chem. 2022, 94, 12274−12279

the manuscript. B.Z. and S.S. designed the experiments. B.Z. performed experiments with help from R.L. B.Z. analyzed data with help from Z.C., Y.X., and J.S. B.Z. and S.S. wrote and edited the paper.

Notes

The mass spectrometry proteomics data have been deposited to the ProteomeXchange Consortium via the PRIDE partner repository (http://proteomecentral.proteomexchange.org) with the data set identifier PXD034086.

The authors declare no competing financial interest.

■ ACKNOWLEDGMENTS

This work was supported by the National Key Research and Development Program of China (2019YFA0905200), National Natural Science Foundation of China (91853123, 81773180, 32101192, 21705127, and 81800655), and China Postdoctoral Science Foundation (2019TQ0260 and 2019M663798).

■ REFERENCES

(1) Watanabe, Y.; Allen, J. D.; Wrapp, D.; Mclellan, J. S.; Crispin, M. *Science* **2020**, *369* (6501), 330−333.
(2) Sztain, T.; Ahn, S. H.; Bogetti, A. T.; Casalino, L.; Goldsmith, J. A.; Seitz, E.; McCool, R. S.; Kearns, F. L.; Acosta-Reyes, F.; Maji, S.; Mashayekhi, G.; McCammon, J. A.; Ourmazd, A.; Frank, J.; McLellan, J. S.; Chong, L. T.; Amaro, R. E. *Nat. Chem.* **2021**, *13* (10), 963−969.
(3) Walls, A. C.; Park, Y. J.; Tortorici, M. A.; Wall, A.; McGuire, A. T.; Veesler, D. *Cell* **2020**, *181* (2), 281−292.
(4) Casas-Sanchez, A.; Romero-Ramirez, A.; Hargreaves, E.; Ellis, C. C.; Grajeda, B. I.; Estevao, I. L.; Patterson, E. I.; Hughes, G. L.; Almeida, I. C.; Zech, T.; Acosta-Serrano, A. *mBio* **2022**, *13* (1), e03718−e03721.
(5) Yang, J.; et al. *Nature* **2020**, *586* (7830), 572−577.
(6) Brun, J.; Vasiljevic, S.; Gangadharan, B.; Hensen, M.; A, V. C.; Hill, M. L.; Kiappes, J. L.; Dwek, R. A.; Alonzi, D. S.; Struwe, W. B.; Zitzmann, N. *ACS Cent. Sci.* **2021**, *7* (4), 586−593.
(7) Sztain, T.; Ahn, S.-H.; Bogetti, A. T.; Casalino, L.; Goldsmith, J. A.; Seitz, E.; McCool, R. S.; Kearns, F. L.; Acosta-Reyes, F.; Maji, S.; Mashayekhi, G.; McCammon, J. A.; Ourmazd, A.; Frank, J.; McLellan, J. S.; Chong, L. T.; Amaro, R. E. *Nat. Chem.* **2021**, *13* (10), 963−968.
(8) Casalino, L.; Gaieb, Z.; Goldsmith, J. A.; Hjorth, C. K.; Dommer, A. C.; Harbison, A. M.; Fogarty, C. A.; Barros, E. P.; Taylor, B. C.; McLellan, J. S.; Fadda, E.; Amaro, R. E. *ACS Cent. Sci.* **2020**, *6* (10), 1722−1734.
(9) Shajahan, A.; Supekar, N. T.; Gleinich, A. S.; Azadi, P. *Glycobiology* **2020**, *30* (12), 981−988.
(10) Wang, D.; Baudys, J.; Bundy, J. L.; Solano, M.; Keppel, T.; Barr, J. R. *Anal. Chem.* **2020**, *92* (21), 14730−14739.
(11) Yao, H.; Song, Y.; Chen, Y.; Wu, N.; Xu, J.; Sun, C.; Zhang, J.; Weng, T.; Zhang, Z.; Wu, Z.; Cheng, L.; Shi, D.; Lu, X.; Lei, J.; Crispin, M.; Shi, Y.; Li, L.; Li, S. *Cell* **2020**, *183* (3), 730−738.
(12) Sanda, M.; Morrison, L.; Goldman, R. *Anal. Chem.* **2021**, *93* (4), 2003−2009.
(13) Zhang, Y.; Zhao, W.; Mao, Y.; Chen, Y.; Wang, S.; Zhong, Y.; Su, T.; Gong, M.; Du, D.; Lu, X.; Cheng, J.; Yang, H. *Proteomics* **2021**, *20*, 100058.
(14) Antonopoulos, A.; Broome, S.; Sharov, V.; Ziegenfuss, C.; Easton, R. L.; Panico, M.; Dell, A.; Morris, H. R.; Haslam, S. M. *Glycobiology* **2021**, *31* (3), 181−187.
(15) Wang, Y.; Wu, Z.; Hu, W. H.; Hao, P. L.; Yang, S. *ACS Omega* **2021**, *6* (24), 15988−15999.
(16) Huang, J.; Wang, D.; Shipman, R. D.; Zhu, Z.; Liu, Y.; Li, L. *Anal. Bioanal. Chem.* **2021**, *413* (29), 7295−7303.
(17) Allen, J. D.; Chawla, H.; Samsudin, F.; Zuzic, L.; Shivgan, A. T.; Watanabe, Y.; He, W. T.; Callaghan, S.; Song, G.; Yong, P.; Brouwer, P. J. M.; Song, Y.; Cai, Y.; Duyvesteyn, H. M. E.; Malinauskas, T.; Kint, J.; Pino, P.; Wurm, M. J.; Frank, M.; Chen, B.; Stuart, D. I.; Sanders, R. W.; Andrabi, R.; Burton, D. R.; Li, S.; Bond, P. J.; Crispin, M. *Biochemistry* **2021**, *60* (27), 2153−2169.
(18) Wang, Q.; Wang, Y.; Yang, S.; Lin, C. Y.; Aliyu, L.; Chen, Y. Q.; Parsons, L.; Tian, Y.; Jia, H. P.; Pekosz, A.; Betenbaugh, M. J.; Cipollo, J. F. *Front Chem.* **2021**, *9*, 735558.
(19) Gstottner, C.; Zhang, T.; Resemann, A.; Ruben, S.; Pengelley, S.; Suckau, D.; Welsink, T.; Wuhrer, M.; Dominguez-Vega, E. *Anal. Chem.* **2021**, *93* (17), 6839−6847.
(20) Lenza, M. P.; Oyenarte, I.; Diercks, T.; Quintana, J. I.; Gimeno, A.; Coelho, H.; Diniz, A.; Peccati, F.; Delgado, S.; Bosch, A.; Valle, M.; Millet, O.; Abrescia, N. G. A.; Palazon, A.; Marcelo, F.; Jimenez-Oses, G.; Jimenez-Barbero, J.; Arda, A.; Ereno-Orbea, J. *Angew. Chem.* **2020**, *132* (52), 23971−23979.
(21) Shen, J.; Jia, L.; Dang, L.; Su, Y.; Zhang, J.; Xu, Y.; Zhu, B.; Chen, Z.; Wu, J.; Lan, R.; Hao, Z.; Ma, C.; Zhao, T.; Gao, N.; Bai, J.; Zhi, Y.; Li, J.; Zhang, J.; Sun, S. *Nat. Methods* **2021**, *18* (8), 921−929.
(22) Haga, Y.; Uemura, M.; Baba, S.; Inamura, K.; Takeuchi, K.; Nonomura, N.; Ueda, K. *Anal. Chem.* **2019**, *91* (3), 2247−2254.
(23) Nakano, M.; Mishra, S. K.; Tokoro, Y.; Sato, K.; Nakajima, K.; Yamaguchi, Y.; Taniguchi, N.; Kizuka, Y. *Mol. Cell. Proteomics* **2019**, *18* (10), 2044−2057.
(24) Miwa, H. E.; Song, Y.; Alvarez, R.; Cummings, R. D.; Stanley, P. *Glycoconj. J.* **2012**, *29* (8), 609−618.
(25) Kizuka, Y.; Taniguchi, N. *Glycoconj. J.* **2018**, *35* (4), 345−351.
(26) Zhao, P.; Praissman, J. L.; Grant, O. C.; Cai, Y.; Xiao, T.; Rosenbalm, K. E.; Aoki, K.; Kellman, B. P.; Bridger, R.; Barouch, D. H.; Brindley, M. A.; Lewis, N. E.; Tiemeyer, M.; Chen, B.; Woods, R. J.; Wells, L. *Cell Host & Microbe* **2020**, *28* (4), 586−601.
(27) Mucha, E.; Lettow, M.; Marianski, M.; Thomas, D. A.; Struwe, W. B.; Harvey, D. J.; Meijer, G.; Seeberger, P. H.; von Helden, G.; Pagel, K. *Angew. Chem.* **2018**, *57* (25), 7440−7443.
(28) Tsuchida, A.; Okajima, T.; Furukawa, K.; Ando, T.; Ishida, H.; Yoshida, A.; Nakamura, Y.; Kannagi, R.; Kiso, M.; Furukawa, K. *J. Biol. Chem.* **2003**, *278* (25), 22787−22794.
(29) Miyazaki, K.; Ohmori, K.; Izawa, M.; Koike, T.; Kumamoto, K.; Furukawa, K.; Ando, T.; Kiso, M.; Yamaji, T.; Hashimoto, Y.; Suzuki, A.; Yoshida, A.; Takeuchi, M.; Kannagi, R. *Cancer. Res.* **2004**, *64* (13), 4498−4505.
(30) Doores, K. J.; Bonomelli, R.; Harvey, R. J.; Vasiljevic, R.; Dwek, R. A.; Burton, R. R.; Crispin, M.; Scanlan, R. N. *Proc. Natl. Acad. Sci. U. S. A.* **2010**, *107* (31), 13800−13805.
(31) Cao, L. W.; Diedrich, J. K.; Kulp, D. W.; Pauthner, M.; He, L.; Park, S. K. R.; Sok, D.; Su, C. Y.; Delahunty, C. M.; Menis, S.; Andrabi, R.; Guenaga, J.; Georgeson, E.; Kubitz, M.; Adachi, Y.; Burton, D. R.; Schief, W. R.; Yates, J. R.; Paulson, J. C. *Nat. Commun.* **2017**, *8*, 14954.

https://doi.org/10.1021/acs.analchem.2c02265
Anal. Chem. 2022, 94, 12274−12279